Journal of Membrane Science 527 (2017) 180–190

Contents lists available at ScienceDirect

Journal of Membrane Science

journal homepage: www.elsevier.com/locate/memsci

Multiscale molecular simulations of the formation and structure of polyamide membranes created by interfacial polymerization

J. Muscatello[a], E.A. Müller[a,*], A.A. Mostofi[b], A.P. Sutton[c]

[a] Department of Chemical Engineering and the Thomas Young Centre for Theory and Simulation of Materials, Imperial College London, Exhibition Road, London SW7 2AZ, United Kingdom

[b] Department of Materials and Department of Physics and the Thomas Young Centre for Theory and Simulation of Materials, Imperial College London, Exhibition Road, London SW7 2AZ, United Kingdom

[c] Department of Physics and the Thomas Young Centre for Theory and Simulation of Materials, Imperial College London, Exhibition Road, London SW7 2AZ, United Kingdom

ABSTRACT

Large scale molecular simulations to model the formation of polyamide membranes have been carried out using a procedure that mimics experimental interfacial polymerization of trimesoyl chloride (TMC) and metaphenylene diamine (MPD) monomers. A coarse-grained representation of the monomers has been developed to facilitate these simulations, which captures essential features of the stereochemistry of the monomers and of amide bonding between them. Atomic models of the membranes are recreated from the final coarse-grained representations.

Consistent with earlier treatments, membranes are formed through the growth and aggregation of oligomer clusters. The membranes are inhomogeneous, displaying opposing gradients of trapped carboxyl and amine side groups, local density variations, and regions where the density of amide bonding is reduced as a result of the aggregation process. We observe the interfacial polymerization reaction is self-limiting and the simulated membranes display a thickness of 5–10 nm. They also display a surface roughness of 1–4 nm. Comparisons are made with recently published experimental results on the structure and chemistry of these membranes and some interesting similarities and differences are found.

1. Introduction

The use of polymer membranes is one of the most promising routes to separating mixtures of global significance [1]. Desalination and the economical purification of large volumes of water are among the greatest challenges the world faces [1]. This is commonly done by reverse osmosis, where a pressure gradient is applied across a membrane allowing water to flow preferentially, leaving behind the impurities, such as ions in the case of desalination. The crux of the process is the membrane itself. Among the many materials choices, a common morphology is an asymmetric composite membrane, where a highly crosslinked polyamide (PA) thin layer is formed by interfacial polymerization on a porous support [2]. In this system, the separation of the water from ions occurs in a thin layer which may be only a few nanometers thick.

Membrane thickness, chemical composition, cross-linking structure and surface roughness are all important properties that are highly dependent on the conditions at which the interfacial polymerization is carried out and are difficult to predict [3]. Furthermore, in spite of the decades of progress in the development and optimisation of PA membranes, little is known about the detailed molecular mechanisms involved in the transport of water through them, largely because the experimental characterisation of polymer films at nanometer scales is very difficult.

Molecular modelling has the potential to shed light on the process of the formation of the membrane through interfacial polymerization, the properties of the membrane itself and on the transport processes of water and ions through it. The decisive point however is to produce a reliable molecular model for the system both in terms of the morphology of the cross-linked polymer and in terms of the reliability of the atomistic force fields employed [4]. While the latter is rather well accepted by the use of “standard” intermolecular potentials, for the former (i.e. setting up a model structure of the networked polymer) there is much more scope for debate.

If one believes that the polymerization process itself has no influence on the morphology of the resulting structure, then the

* Corresponding author.
E-mail address: e.muller@imperial.ac.uk (E.A. Müller).

http://dx.doi.org/10.1016/j.memsci.2016.11.024
Received 2 September 2016; Received in revised form 30 October 2016; Accepted 13 November 2016
Available online 24 November 2016
0376-7388/

process of building a model of the membrane reduces to postulating an arrangement which is both chemically sound and a stable equilibrated atomistic configuration. For the case of the PA membranes the idealized chemical structure corresponds to a highly cross-linked polymer matrix with a known stoichiometry.

Roux et al. [5] have built virtual membranes by progressively bonding the constituent solvent-free monomeric species on the basis of a heuristic distance criterion during MD simulations until the system interconnectivity reaches completion and a target (experimental) density is achieved. Realizations of membrane models of this type [6–9], with different heuristic protocols and annealing procedures have been used these to study the transport of water and ions. Colina et al. [10] have progressed these ideas by championing the use of a systematic algorithm [11] that combines chemical moieties in a virtual environment in an ad-hoc randomized way. This produces cross-linked polymers model structures with predetermined properties that can later be employed in studying transport and/or structural properties. This process has also been used to produce PA model membranes [12].

Instead of starting off with monomer units, one could consider only a packing of linear oligomers. However, this produces membranes with significantly different characteristics from those that are cross-linked and at odds with experimental information [13,14]. Nevertheless, suitably packed collections of linear chains have been employed as building blocks for PA membrane models [15–17]. Hughes and Gale [18] cross-link pre-formed linear polymer chains, each consisting of 23 repeat units, by solvating them in water and randomly bonding carboxylic acid groups that were 5–9 Å apart to generate a cross-linked polymer layer. An interesting aspect of this work is that the authors considered explicitly the effect of the support layer and compared in their simulations a free-standing thin film with films supported on a flat porous or non-porous substrates. An important outcome of the work of Hughes and Gale is that they observe no influence of the presence of the substrates on their simulations. Ding et al. [19–21] further employ the conceptual idea of artificially cross-linking linear polymer segments as a methodology to create appropriate membrane models.

In spite of the apparent success implied by the agreement between the above mentioned models and the limited atomistic level characterization available for PA membranes, there is still the lingering question as to the faithfulness of these ad-hoc models to provide a reliable picture of the molecular details of relevance to the transport of fluids across PA membranes. One would expect that a “mimetic” or evolutionary approach, based on a model that mimics the formation of the real material, would provide the most accurate representation of the membrane molecular structure. This approach has been championed in other areas of materials science and has proven to be successful in producing models of activated carbons [22] and porous materials for adsorption [23]. The issue with the mimetic production of an interfacial polymerization membrane by simulation is that the time frames for the experimental process are many orders of magnitude larger than those accessible by molecular modelling. To our knowledge, the first attempt to adopt a mimetic approach was the work of Nadler and Srebnik [24], who employed a cluster-cluster aggregation scheme to simulate dynamically the formation of a PA membrane from the constituent monomers. The membrane model produced, albeit a coarse-grained (CG) representation, gave insights into the kinetics of formation and the structure of the membrane, but lacked the atom-level detail needed for the description of water and ion transport. CG models, where some degrees of freedom have been removed, provide a means to access longer time scales than do conventional MD simulations and have been explored as a means to generate plausible configurations by interfacial polymerization. In particular dissipative particle dynamics (DPD) has the appropriate level of integration that allows the merging of groups of molecules into “blobs” of matter while removing the explicit effect of the solvent. DPD, however does not account for the kinetics of the reaction, which must be added artificially. Berezkin and Kudryavtsev [25–27] have recently reported a hybrid adaptation of DPD with larger scale continuum finite difference methods. The results obtained provide a quantitative picture of the effects of cross-linking of the polymer, adding to the picture that the degree of cross-linking has a profound effect on the morphology of the membrane, as it disallows the movement of the monomeric species in the core of the polymer matrix producing a strongly heterogeneous environment. On the other hand, fully analytical models (e.g. Ref. [28]) fail to describe the molecular level detail that is crucial to understanding the transport processes of water and ions through these inhomogeneous membranes.

In spite of the above progress, it is clear that current computational resources are insufficient to simulate in atomic detail either the polymerization process or transport processes in realistic system sizes and experimental timescales. Despite advances in parallel processing and algorithms, the use of graphical processing units and the reduction in costs of hardware, these computational limits are bound to remain essentially unchanged (see the comments made during a Faraday Discussion on the topic [29]) in the near future. In this paper we describe a way around this limitation by means of a multi-scale modelling technique where we model the interfacial polymerization process using a coarse-grained representation which retains the shape and connectivity of the underlying monomers, while emulating diffusion of monomers through their solvents without treating the solvents explicitly. We are then able to map these CG models onto fully atomic configurations through a further relaxation procedure. In this way the underlying physical processes involved in the interfacial polymerization are captured faithfully, including the conformationally correct bonding during polymerization and the aggregation of polymer clusters while ultimately reporting atomically detailed models of membranes.

The paper is organised as follows. In Section 2 the experimental procedure for creating membranes by interfacial polymerization is reviewed to identify the processes that should be included in a realistic simulation. The coarse-grained representations of the MPD and TMC monomers, their reaction products and the simulation protocol are described. The results in Section 3 begin with the mechanism and kinetics of the formation of the membranes through the growth and aggregation of clusters. The atomic structures of membranes formed from three different ratios of concentrations of the two reactant monomer species are presented alongside maps of amide bonds and amine and carboxyl side groups within them. Similar atomic structures and maps are also presented for a variety of oligomer cluster sizes prior to their incorporation in the membranes. The discussion in Section 4 contains comparisons with earlier simulations and experiments of dry and hydrated membranes and in particular with the recent experiments of Karan et al. [30].

2. Method

2.1. Overview of experimental procedure

Thin-film composite PA membranes are experimentally manufactured by interfacial polymerization, as first documented in 1959 by Morgan et al. [31,32]. In this process two reactive species undergo a polymerization reaction at the interface between two immiscible solvents [33]. Typically these reactants consist of an amine and an acid chloride dissolved in an aqueous and organic solvent respectively. A microporous backing, typically polysulfone, is immersed in the aqueous solution containing the amine reactant. This backing film is brought into contact with the organic solution of acid chloride. The amine component diffuses into the organic solvent, but the acid chloride is almost insoluble in water and remains in the organic solvent. As a result, the polymerization reaction takes place in the organic solvent at and near the interface between the two solvents. The reaction is self-limiting because the precipitating PA becomes a barrier to the intermixing of the reactants. A common choice of reactants for reverse

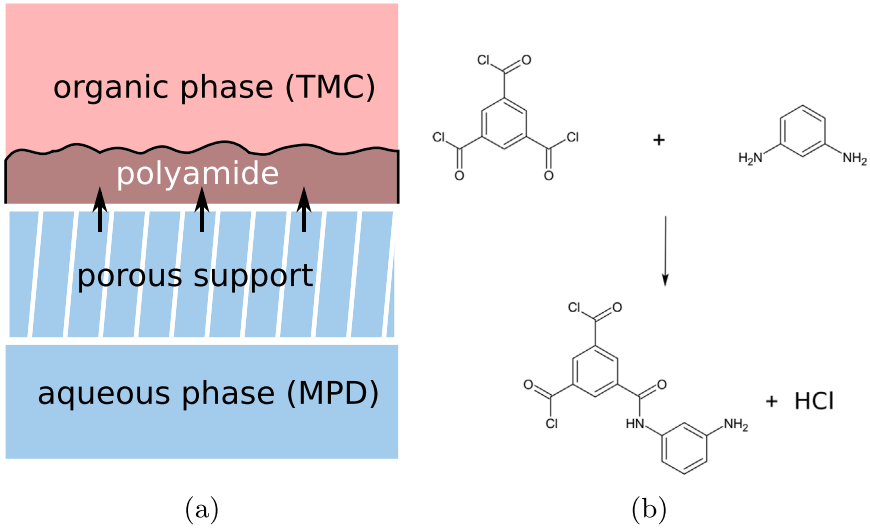

Fig. 1. (a) Schematic diagram of the experimental procedure for the production of a PA membrane via interfacial polymerization. The arrows depict the flux of MPD monomers into the organic phase. (b) Chemical reaction of metaphenyline diamine (left) and 1,3,5-trimesoyl chloride (right) monomers to produce a PA oligomer and HCl.

osmosis membranes is metaphenyline diamine (1,3-benzenediamide or MPD) and trimesoyl chloride (1,3,5-benzenetricarbonyl chloride or TMC). This combination, which forms part of the composite membrane industrially known as FT30 [34], is capable of up to 99.5% salt rejection, while admitting a high flux and exhibiting good mechanical properties [35]. A schematic of the experimental procedure is shown in Fig. 1a. The corresponding chemical reaction between two monomers is shown in Fig. 1b, where it is seen that hydrochloric acid is released by the reaction. For further details the reader is referred to standard textbooks (e.g. Ref. [36]), while a critical review of the state-of-the-art is given by Wang et al. [37].

In this work molecular dynamics simulations of the formation of PA membranes are presented that attempt to mimic the above experimental procedure as closely as possible. This is facilitated through the use of coarse-grained representations of the reactant monomers, which are described in the next section.

2.2. Coarse-grained representations of the monomers and their reaction products

To reduce the number of force computations a coarse-grained (CG) model is used to represent the component monomers and resulting oligomers. The aim of this approach is to create a representation that polymerizes in such a way that the bond lengths and molecular conformations correspond to those of a realistic atomic structure while reducing the number of internal degrees of freedom, as illustrated schematically in Fig. 2.

The benzene ring of each monomer is replaced by a triad of beads at the vertices of a rigid equilateral triangle with sides of length 2.42 Å. The orientations and lengths of the bonds to the side groups are also rigid. They emanate from the vertices, B, of the triangles and they are coplanar with the triangles. Let B_M be the (carbon) site in MPD to which an amine side group is bonded. The length of the B_M–N bond is fixed at 1.42 Å. Let B_T be the (carbon) site in TMC to which an acyl chloride side group is bonded. The length of the B_T–C bond is fixed at 1.51 Å. The side groups are free to rotate about the B_M–N and B_T–C bonds. As a result of this rotational freedom the N–H bonds in MPD and C–Cl bond in TMC lie on the surfaces of two cones, as depicted in Fig. 2. The apex angle of each cone is set to 120°. Conversely, once an amide bond is formed between TMC and MPD (Fig. 2 bottom panel) the orientations of the B_M–N and B_T–C bonds become fixed to accord with the known planarity of the amide bond.

By ensuring that each amine side group may form only one amide bond the representation simulates the steric hindrance that exists in the real system, which prevents two amide bonds to a single nitrogen atom. The reaction involves the removal of a hydrogen atom attached to the nitrogen in an amine side group of MPD and the removal of the chlorine atom in an acyl chloride side group of TMC, see Fig. 1b. This enables the carbon atom in the acyl chloride side group to form an amide bond (sometimes called a peptide bond) to the nitrogen atom in the amine side group. The HCl generated by the reaction is discarded. In the simulations the reaction happens when the distance between the carbon atom of an acyl chloride side group and the nitrogen atom of an amine group is less than 2.375 Å, which is 1 Å greater than the C–N bond length in the amide bond.

The bond length for the C–N amide bond was determined by finding the minimum energy configuration of a TMC-MPD oligomer using density functional theory (DFT) at the B3LYP/6–31G* level of theory [38–40]. In particular, the equilibrium bond length between the carbon and nitrogen atoms is found to be 1.375 Å. The atomic structures of the amide bond and the amine and acyl chloride side

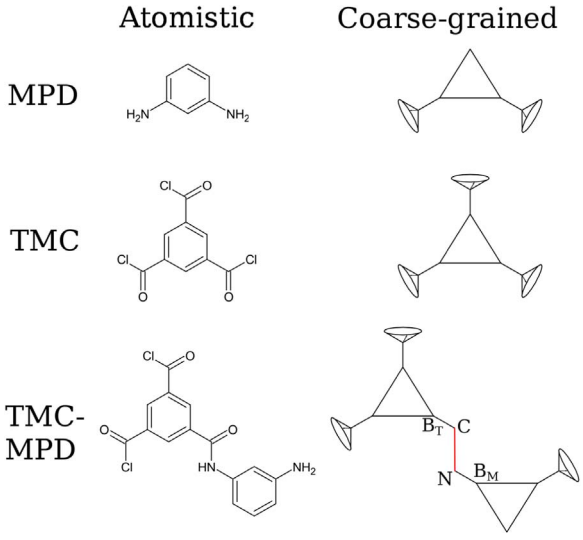

Fig. 2. Left column: Atomic structures of MPD and TMC monomers and an MPD-TMC oligomer. Right column: corresponding coarse-grained representations (not to scale). The amide bond in the oligomer is shown in red. The N–H bonds in the amine side groups and the C–Cl bonds in the acyl chloride side groups lie on the surfaces of cones with apex angles of 120°. These bonds are along the directions of possible C–N amide bonds, shown as broken lines in Fig. S9b. (For interpretation of the references to color in this figure legend, the reader is referred to the web version of this article).

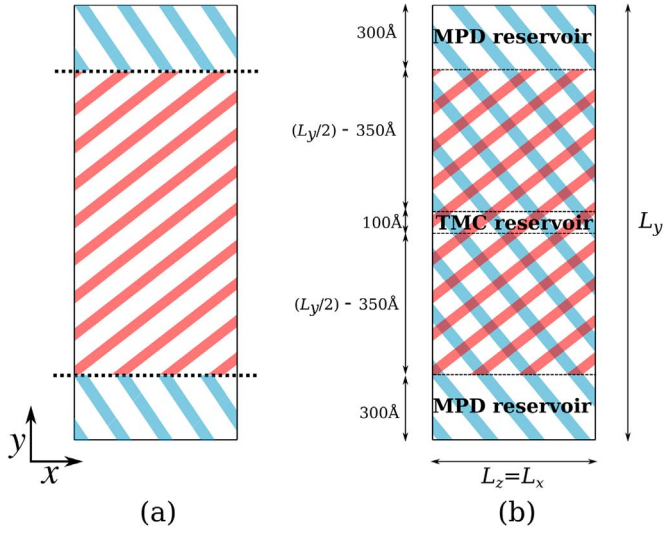

Fig. 3. (a) Initial distribution of TMC (red shading) and MPD (blue shading) monomers in the computational cell before interfacial polymerization reactions are allowed to take place. The thick broken lines represent grids of repulsive potentials to keep the TMC and MPD monomers apart. (b) Following initial equilibration the repulsive interactions between the grids and MPD monomers are switched off. This allows MPD monomers to leave the region where they were confined and diffuse throughout the computational cell. TMC monomers continue to be confined to the region shown in (a). The locations of reservoirs of MPD and TMC monomers are shown by thin broken lines. When MPD monomers come into contact with TMC monomers polymerization reactions take place at and near the thick dotted lines. Eventually spanning membranes are formed parallel to *x* and *z* (*z* is out of the page). The concentrations of MPD and TMC monomers in the reservoirs are maintained approximately constant throughout the simulation by continuous insertions. Periodic boundary conditions are applied to all faces of the computational cell. (For interpretation of the references to color in this figure legend, the reader is referred to the web version of this article).

groups, as determined by DFT, are detailed in the Supplementary material.

The amide bond should be coplanar with the bonds B_T–C and B_M–N connecting the carbon and nitrogen atoms to the two benzene rings, as shown in fig S9a. It is essential to maintain this coplanarity to avoid spurious polymerized configurations. The bond angles B_T–C–N and C–N–B_M are approximated as 120°. The coplanarity could be achieved by introducing a B_T–C–N–B_M torsion potential, but it would have to be supplemented by a bond-stretching potential to give the correct amide bond length. A detailed analysis of the algorithms and procedures to enforce the appropriate atomistic structures is given in the Supplementary material.

The non-bonding interaction between monomers is approximated by Lennard-Jones potentials acting between the vertices, B, of the equilateral triangles representing benzene rings on different monomers. The parameters are closely related to the SAFT-γ force-field parameters for interactions between benzene rings [41]. At long range, monomers interact only through these Lennard-Jones potentials, however, at short range these potentials are supplemented by purely repulsive interactions between side groups of the same kind to avoid spurious overlaps. The parameters for the non-bonding potentials and further details are given in Table S1 of the Supplementary material.

2.3. Langevin dynamics

To reduce computational time associated with diffusion of monomers through the solvents Langevin dynamics [42] is used to model their transport, thereby avoiding the explicit use in the simulation of any solvent. This is an essential step to render the simulations tractable with current computer hardware. This approach is similar to that used previously to investigate the dynamics and self assembly of patchy colloids [43].

The Langevin equation of motion for the translational degrees of freedom of the *i*th monomer is as follows: [21,44]

$$\mathbf{F}_i(t) = -\nabla_i U - \gamma_i \mathbf{v}_i(t) + \sqrt{2k_B T\gamma_i}\,\mathbf{R}_i(t), \tag{1}$$

where U is the total potential energy of the system comprising the monomers and their interactions, ∇_i is the gradient operator with respect to the centre of mass of monomer i, $\mathbf{v}_i(t)$ is the velocity of monomer i, k_B is the Boltzmann constant, T is the temperature, γ_i is a friction coefficient that depends on whether the monomer is TMC or MPD, and $\mathbf{R}_i(t)$ is a random force acting on monomer i, each Cartesian component α of which satisfies $\langle R_{i\alpha}(t)\rangle=0$ and $\langle R_{i\alpha}(t)R_{i\alpha}(t')\rangle=\delta(t-t')$. The random force simulates the buffeting of each monomer by solvent molecules, and it is related through the fluctuation-dissipation theorem to the friction force the monomer experiences in the solvent. If m_i is the mass of monomer i there is a relaxation time $\tau=m_i/\gamma_i$ due to the interaction with the implicit solvent.

The rotational degrees of freedom are propagated by integrating the following equation of motion for the α-component of the angular velocity $\boldsymbol{\omega}_i$ of monomer i [22]:

$$I_{\alpha\alpha}\omega_{i\alpha}(t) = -\frac{\partial U}{\partial \omega_{i\alpha}} - \zeta_{i\alpha}\omega_{i\alpha}(t) + \sqrt{2k_B T\zeta_{i\alpha}}\,R_{i\alpha}(t), \tag{2}$$

where I is the diagonalised inertia tensor, and $\zeta_{i\alpha}$ is the friction coefficient for rotational motion of the ith monomer. The relaxation time associated with this friction coefficient is $I_{\alpha\alpha}/\zeta_{i\alpha}$.

In this work, the Langevin equations of motion of monomers are integrated using the LAMMPS molecular dynamics routine that treats monomers as rigid particles [45], solving for the three rotational and three translational degrees of freedom associated with each monomer. A relaxation time of 2 ps is chosen for all degrees of freedom by adjusting the friction coefficients at the beginning of the simulation. Approximating a monomer as a spherical particle of radius R and mass M and using Stokes' law [46], the viscosity of the solvent is given by

$$\eta_{solvent} = \frac{M}{6\pi\tau R} \tag{3}$$

For M≈100 amu and R≈5 Å, we obtain $\eta_{solvent}\approx 10^{-5}$ Pa s. This is an order of magnitude smaller than that of hexane [47] ($\eta_{hexane}=3.0\times10^{-4}$ Pa s). By using this smaller viscosity we are able to enhance the diffusivity of monomers in the solvents, leading to more polymerization reactions for a given duration of simulation.

2.4. Simulation setup

The simulations aim to mimic the experimental procedure for synthesizing the PA films as closely as possible. The two monomer species are initially confined to separate regions in the rectangular computational cell, as illustrated in Fig. 3a, simulating the immiscibility of the solvent phases. This separation is effected by two two-dimensional grids of purely repulsive interactions in *x*–*z* planes spanning the computational cell, between slabs where MPD and TMC monomers are initially confined. These grids are shown as thick black lines in Fig. 3. The grid points interact selectively with benzene rings of the monomers via repulsive WCA potentials. After an equilibration period of 5 ns, the repulsive interactions between the grid points and MPD monomers are turned off, allowing MPD monomers to leave the region where they are initially confined and enter the region where TMC continues to be confined. Two interfacial regions are present in the system due to the periodic boundary conditions, leading to the formation of two independent membrane configurations, as shown schematically in Fig. 3b.

As the polymerization reactions proceed and consume monomers, further monomers diffuse towards the reaction zones, driven by the concentration gradients. To mimic the presence of bulk regions far from the interfaces, where the concentrations of monomers are constant, regions within the computational cell are designated as

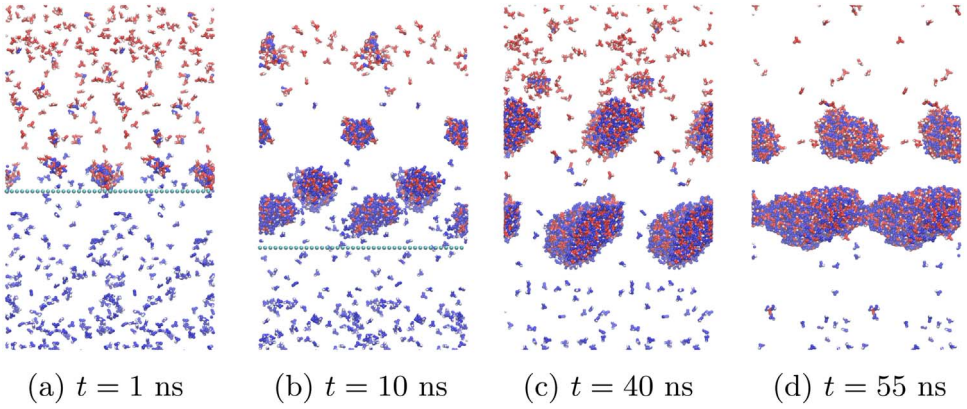

Fig. 4. Snapshots at successive times of a coarse-grained simulation of the formation of a spanning membrane with c_{MPD}:c_{TMC}=3:2 in a larger computational cell size of L_x=L_z=100 Å, L_y=2000 Å. Each snapshot shows two repeat periods for clarity, so each snapshot is 20 nm from left to right. TMC monomers are shown in red and white and MPD monomers are in blue and white. In (a) and (b) the line of green spheres show the location of the interface between the immiscible solvents. The contents of the computational cell drift rigidly together because total momentum is not conserved with Langevin dynamics. Note the local reduction in the numbers of free monomers with computational time and the very small monomer concentration between clusters. (For interpretation of the references to color in this figure legend, the reader is referred to the web version of this article).

reservoirs with approximately constant number density of the monomers. As monomers diffuse from the reservoirs to the reaction zones, they are replaced at random sites (but avoiding sites of existing monomers) and in random orientations in the reservoir. The LAMMPS molecular dynamics code was modified in-house for this purpose. In this way, the system resembles a simplified version of the dual-control volume method [48] to maintain regions of differing chemical potential.

Three ratios c_{MPD}:c_{TMC} of the numbers of MPD to TMC monomers per unit volume in the reservoirs are investigated, equal to 1:1, 3:2, and 3:1, all sharing the same MPD concentration used commonly in experiments of 2 wt% in aqueous solution [11,49]. In an aqueous solution of 2 wt% MPD there are approximately 300 water molecules for every MPD monomer, and the mass density of the solution remains approximately 103 kg m^{-3}. If the volume of the MPD reservoir is V_r, expressed in Å^3, to maintain a concentration of 2 wt% MPD in the reservoir requires approximately ($1.1\times10^{-4}\times V_r$) MPD monomers. The size of the computational cell is L_x=L_z=50 Å with L_y=2000 Å for composition ratios of 1:1 and 3:2, and L_y=4000 Å for the 3:1 ratio. The much greater length in the y-direction reduces the migration of monomers and clusters between adjacent computational cells along the y-direction, as a result of the periodic boundary conditions, and thus maintains the independence of the two interfacial polymerization regions within the computational cell.

The simulations are run for at least 90 ns, with a time step of 1 fs. When clusters spanning the computational cell are formed they block further diffusion of MPD into the region occupied by TMC monomers. These spanning clusters then grow extremely slowly through the reaction with monomers at any remaining available surface sites, and the accretion of diffusing clusters trapped between the spanning clusters.

Relaxed atomic configurations are generated from the coarse-grained representations as follows. The amide bonds of the polymerized coarse-grained representation are retained and no new amide bonds are introduced. At each amide bond hydrogen and oxygen atoms are introduced into the planes of the triangles formed by C-N-B_M and B_T-C-N respectively. This is done in such a way that the O–C–B_T, O–C–N, C–N–H and H–N–B_M bond angles are 120°. The rigid triangle of each coarse-grained representation of a benzene ring is replaced by the usual hexagon of carbon atoms and hydrogen atoms, with amine side groups replacing nitrogen atoms that are not part of amide bonds. Surviving acyl chloride groups are assumed to be hydrolyzed and replaced by carboxyl groups. Once the atomic structure is generated it is relaxed by a simulated annealing procedure at 300 K.

Liyana-Arachchi et al. [12] compare the properties of atomistic PA membranes generated with different popular atomistic force-fields concluding that the differences amongst them are not statistically significant. In that sense, and with no prejudice, bonding and non-bonding atomic interactions are provided herein by the AMBER force field [50] with the assumption that these models are transferable. Atomic charges are obtained by adapting those used in the work of Ding et al. [7] so that small bonded groups of atoms remain charge neutral, such as the amide bond, the amine and acyl chloride side groups, the benzene rings and the carboxyl groups. This enables a simple, local approach to be taken to charge transfer while retaining polar groups. The charges applied to atoms in each of these groups are detailed in the Supplementary material, along with links to download configuration files.

3. Results

3.1. The formation of the membranes

Fig. 4 shows a sequence of snapshots of the formation of a membrane. In the early stages (Fig. 4a) MPD monomers (blue and white) are seen entering the region where TMC monomers (red and white) are confined, where some of them react to form small oligomers. Growth by further polymerization and aggregation of oligomers occurs (Fig. 4b and c) and eventually a spanning cluster is formed (Fig. 4d) which continues to grow (Fig. 4d) by the accretion of further monomers at reaction sites and oligomers on the membrane surfaces. The spanning cluster prevents further ingress of MPD monomers into the region occupied by TMC monomers. The rate of growth of the membrane eventually decreases almost to zero (see Fig. 5) as the reaction sites on the surface are exhausted and the remaining oligomer clusters are too remote to diffuse to the membrane in a reasonable time. The simulation is then stopped. The formation of the membrane can be described as a reaction-aggregation process limited by diffusion of the reactants from remote reservoirs [51].

Fig. 5 shows the growth in time of the largest cluster in each half of the computational cell for each of the three composition ratios. It is seen that some of the largest clusters grow at a fairly steady rate through the accretion of monomers and small oligomers, but some grow abruptly through the merging of relatively large clusters. In reality one can expect growth to occur through the accretion of monomers and a distribution of oligomer sizes. The distributions of oligomer sizes in the simulations are limited by the sizes of the computational cells, so no particular significance can be attached to them.

Fig. 6 shows the average number of amide bonds of each monomer

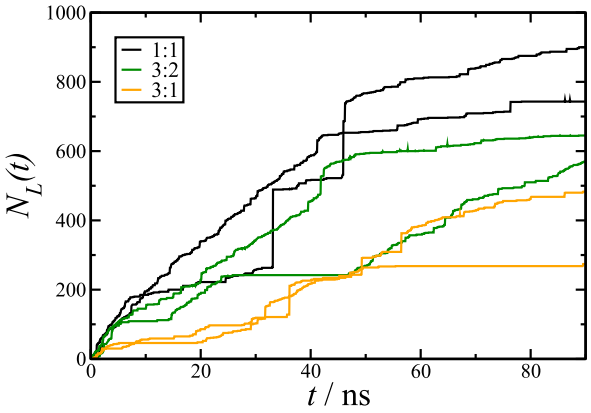

Fig. 5. The increase with time of the number of monomers, N_L, in the largest cluster in each half of the computational cell for all three monomer compositions.

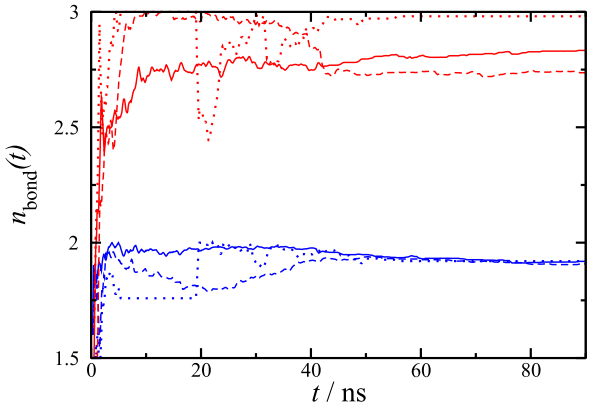

Fig. 6. Average number, n_{bond}, of amide bonds per TMC monomer (red) and per MPD monomer (blue) in the largest cluster as a function of time. Solid lines are for c_{MPD}:c_{TMC}=1:1, dashed lines are for c_{MPD}:c_{TMC}=3:2, and dotted lines are for c_{MPD}:c_{TMC}=3:1. For clarity the data have been smoothed by averaging over intervals of 0.5 ns. The increase with time of the number of monomers, N_L, in the largest cluster in each half of the computational cell for all three monomer compositions. (For interpretation of the references to color in this figure legend, the reader is referred to the web version of this article).

type as a function of time in the largest cluster for each ratio of monomer compositions. If the polymerization reaction were complete each MPD monomer would have two amide bonds and each TMC monomer would have three amide bonds. It is seen in Fig. 6 that the number of amide bonds per MPD monomer reaches a steady value of about 1.9, while the number of amide bonds per TMC monomer reaches values between 2.75 and 3.0 depending on the monomer composition, indicating a degree of cross-linking consistent with X-ray photoelectron spectrometry observations [52,53]. These numbers do not change in the relaxed atomic configurations.

3.2. Atomic structures of the membranes

Fig. 7 shows projections of two repeat periods of the atomic structures of one of the two membranes formed in a computational cell corresponding to a concentration ratio c_{MPD}:c_{TMC} of 1:1, viewed along perpendicular directions in the plane of the membrane. The figures for all six membranes studied are presented in the Supplementary material. In the atomic structures red and blue dots correspond to oxygen and nitrogen atoms respectively. Some membranes have been flipped over to ensure the orientation of each membrane is such that a TMC reservoir is above the upper surface and an MPD reservoir is below the lower surface. To reveal the bonding further there are projections showing only the amide bonds (cyan), the surviving amine groups (dark blue) and the carboxyl groups (red). If a membrane were fully polymerized there would be only amide bonds and no amine groups or carboxyl groups.

There are several common features in these membranes:

- In general, there are more carboxyl groups in the upper half of the membrane and more amine groups in the lower half, reflecting the locations of the TMC and MPD reservoirs relative to the membrane.
- Since the membranes are formed from the aggregation of clusters there is significant surface roughness, in some cases comparable to the thickness of the membrane.
- The degree of polymerization is remarkably high even in some of the promontories at the surfaces of the membranes.
- The thicknesses of the membranes are difficult to define in view of the surface roughness, but the 1 nm scale markers indicate they are between 5 and 10 nm.
- Some membrane surfaces have carboxyl groups on them, some have amine groups and some are almost fully polymerized.
- It is evident that there are significant local variations in the densities of the membranes, with some voids, at the surfaces and even in the middle of the membranes.

Since the membranes are formed from the aggregation of clusters it is instructive to consider the bonding in the clusters and the distribution of their sizes. Soon after MPD monomers enter the region where TMC is confined small oligomer clusters are formed reducing the local concentrations of the monomers (see Fig. 4a). This leads to the formation of opposing concentration gradients of TMC and MPD monomers since the TMC and MPD reservoirs are on opposite sides of the reaction zone. The growth of an oligomer cluster through polymerization reactions depends on the availability of both TMC and MPD monomers. It follows that once concentration gradients are established there will be a distribution of oligomer cluster sizes with maxima in regions where the ratio of concentrations of MPD and TMC is closest to 3:2, and minima in regions where either the MPD or TMC concentrations are very small.

If a cluster is fully polymerized its monomer composition must be $(MPD)_3(TMC)_2$. If the cluster has more TMC there will be an excess of acyl chloride groups, and conversely if it has more MPD there will an excess of amine groups. This explains why there are more carboxyl groups (which come from hydration of the acyl chloride groups) in the upper part of the membranes, and more amine groups in the lower part of the membranes. This asymmetry in the membrane is consistent with experimental contact angle titration studies [54].

Fig. 8a–f shows the relaxed atomic structures of six oligomer clusters and the amide, amine and acyl chloride groups in them. These clusters are formed in the reaction zone outside the membranes. The clusters shown in (a)–(c) are formed in a 1:1 ratio of MPD to TMC, while those shown in (d)–(f) are formed in a 3:1 ratio of MPD to TMC. We have confirmed that in all six cases the amine and acyl chloride groups lie on the surfaces of these clusters. We observe consistently that when clusters have formed from reactions with monomers, and before they have merged with other clusters, the surviving acyl chloride and amine groups lie on the surfaces of the clusters.

When clusters merge with acyl chloride and amine groups on their surfaces, such as those shown in (a)–(c), some of these groups will be able to react to form amide bonds. For steric reasons it is unlikely that all the acyl chloride and amine groups on their surfaces will react because not all of them will be able to approach each other sufficiently closely. When clusters merge with only amine groups on their surfaces, such as those shown in (d)–(f), the amine groups cannot be eliminated because there are no acyl chloride groups for them to react with. A similar situation arises when clusters with excess acyl chloride groups on their surfaces merge; the excess acyl chloride groups cannot be eliminated. Those acyl chloride and amine groups that are unable to react when clusters merge then become trapped at interfaces between the clusters, with excess acyl chloride groups eventually becoming

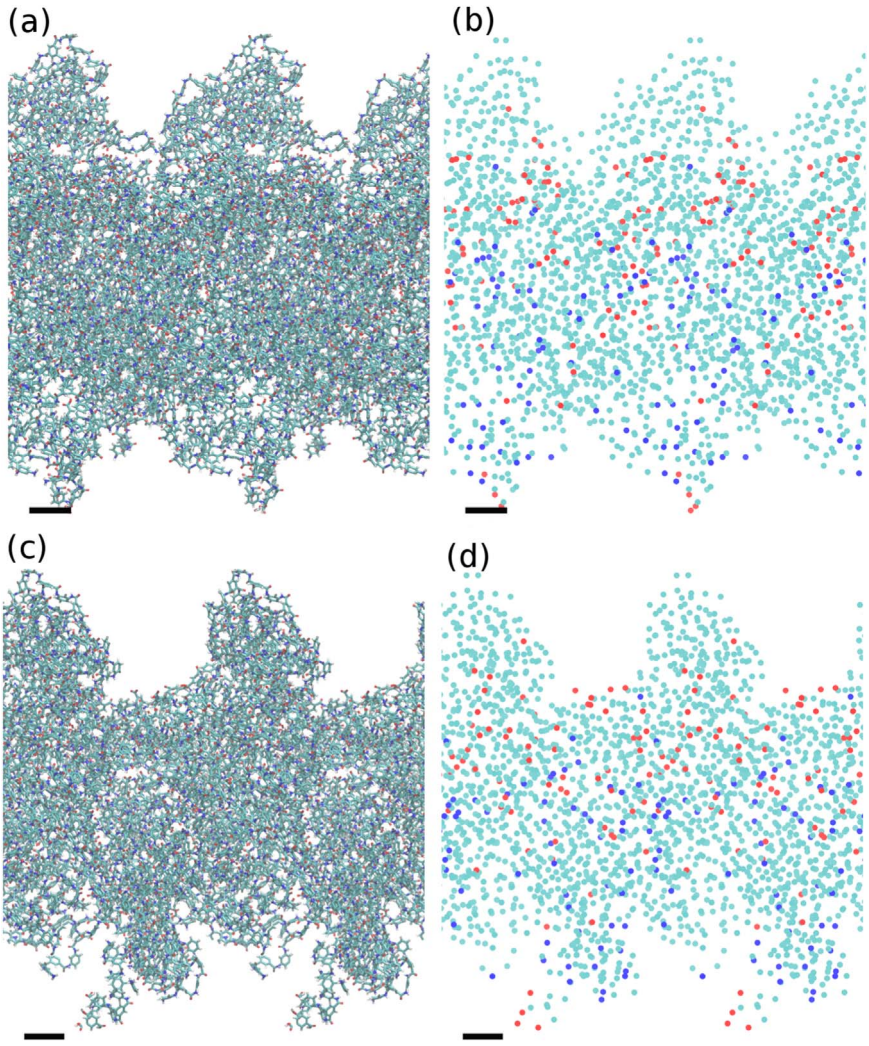

Fig. 7. One of the two membranes formed in the computational cell with a 1:1 composition of MPD:TMC. (a) Projected atomic structure along x, where red dots are oxygen atoms and dark blue dots are nitrogen atoms. (b) The same view as in (a) but showing the nitrogen atoms in amide bonds (cyan), the oxygen atoms in the hydroxyls of the carboxyl groups (red) and the nitrogen atoms in the amine groups (dark blue). Carboxyl groups are assumed to be formed from the remaining acyl chloride groups when the membrane is exposed to water. (c) and (d) are the same as (a) and (b), but viewed along z. The scale bars show 1 nm. (For interpretation of the references to color in this figure legend, the reader is referred to the web version of this article).

carboxyl groups on exposure to water. It follows that the degree of amide bonding between clusters is unlikely to be as high as that within clusters, and that other forms of bonding between clusters may be more significant such as van der Waals and electrostatic interactions.

4. Discussion

The picture for the membranes that emerges from these simulations is that they are inhomogeneous in three principal respects. First, there are opposing concentration gradients of amine and carboxyl groups between the membrane surfaces. Second, the membrane comprises regions where the degree of polymerization is high separated by interfaces where it is relatively low. Third, there are significant variations in the local density, with some voids. These features are a consequence of the formation of the membrane from the aggregation of clusters, which is also responsible for the surface roughness.

The resulting morphology may have a direct bearing on transport of small molecules through the membrane where the weaker bonding across interfaces between former separate clusters may provide channels for easier diffusion. In this limited sense the membrane has a structure analogous to a nanocrystalline material, where almost defect-free nanocrystallites are separated by grain boundaries with less densely packed atomic structures which provide channels for rapid diffusion [55].

4.1. Comparison with other experiments and simulations

The formation of the membrane from the aggregation of oligomer clusters, with a distribution of sizes, appears to be a key feature of interfacial polymerization, as first proposed by Meakin [30]. As we have noted above it is responsible for inhomogeneities in the membrane. The simulations of Nadler and Srebnik [5] were the first to treat this feature explicitly using a coarse-grained representation of the monomers. Their coarse-grained model is significantly simpler than the coarse-grained representation used here. For example, their monomers are modelled as spherical particles, ignoring the positions of the functional side groups, and the conformational constraints on the formation of planar amide bonds that have been treated explicitly here. But despite these simplifications, and a number of others, Srebnik and coworkers [56] also found their membranes had rough surfaces as a result of cluster aggregation and that their membranes were inhomogeneous. However, as far as we know, the work reported in this paper is the first to present *atomic* structures of PA membranes produced by simulated interfacial polymerization.

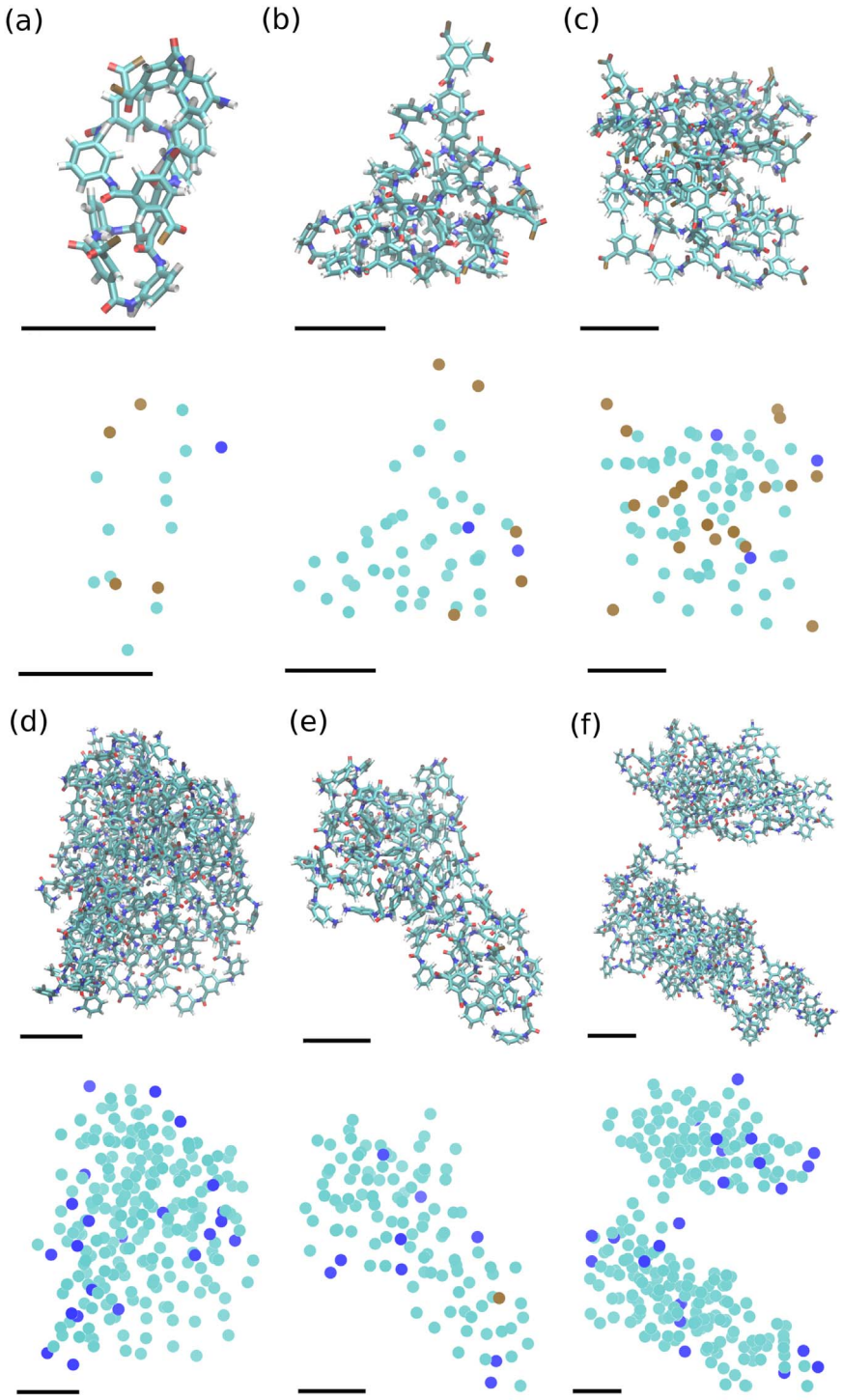

Fig. 8. Relaxed atomic structures of six clusters, (a)–(f), formed outside the membranes. Brown atoms are chlorine, red are oxygen and blue are nitrogen. Beneath each atomic structure is a map of the chemical groups in the cluster: amide (cyan), acyl chloride (brown) and amine (dark blue). (a)–(c) are formed in a 1:1 mixture of MPD:TMC. (d)–(f) are formed in a 3:1 mixture of MPD:TMC. The scale bars are 1 nm. (For interpretation of the references to color in this figure legend, the reader is referred to the web version of this article).

Simulations where the membrane is produced by artificially packing monomers or polymers in an ad-hoc way disregard the actual process of interfacial polymerization and its consequences for the degree of polymerization and cross-linking, the residual densities and distributions of acyl chloride and amine groups in the membranes, and the thickness and surface roughness of the membranes. In spite of this, some properties of the dry (and hydrated) model membranes can be compared directly.

The dry polymer density (before hydration) is a rather ill-defined property, as one must decide to take into consideration the presence or not of voids in the structure and/or the inhomogeneity of the interfaces. This is particularly so in the case of membranes produced by mimicking interfacial polymerization. Some experimental measurements refer to the polymer matrix as a whole (including possible voids) [57] reporting density values of 1.24 g/cm^3 . An upper limit of 1.38 g/cm is suggested [8] corresponding to the linear crystalline version of the PA polymer. Our data range from 1.17 to 1.33 g/cm^3 and average 1.25 g/cm^3 (raw data in Supplementary material) which is a surpris-

ingly accurate match to experimental data, considering this is a prediction of the model. Available data for other membrane models reported in the literature span 1.17 g/cm^3 [7] to 1.31 g/cm^3 [12], again commensurate with our models.

4.2. Comparison with hydrated membranes

A comparison is made between the hydration of the membranes produced and counterparts reported in the literature. The membranes are hydrated using the following procedure: SPC/E water [58] is initially introduced into the system cell by placing molecules on a regular lattice, avoiding overlaps with the membrane and with an initial density close to 1 g/cm^3. The system is then run for 1 ns using the NPT Nosé-Hoover barostat with a pressure of 100 bar and 300 K and a timestep of 1fs; due to the anisotropic barostat, the cell contracts along the y direction as water molecules enter the membrane. Although we are interested in the conditions at atmospheric pressure in order to compare to experiments, a higher pressure is applied in order to speed up the process of water diffusion in the membrane. After this period, the system is allowed to reach equilibrium at a pressure of 1 bar in the y-direction (perpendicular to the membrane surface). The system is deemed to have reached equilibrium when the system cell has stopped contracting in volume. For the membranes generated in this work, an equilibration time of at least 10 ns was required.

The hydrated membrane absorbs a significant amount of water, as seen in Fig. 9, where polymer and water profiles are plotted in the direction transverse to the membrane. Upon hydration, the density of the solvent-free polymer drops but the distribution of mass does not spread out uniformly. It seems that the observed swelling (i.e. spreading out of the density profile) mainly occurs at the surface regions with a average estimated value of 8% (range from 3.8% to 13.4%). The implication is that the water uptake is not uniform, being largest in the promontories of the surface roughness and smallest in the middle of the membrane [6]. Water uptake is on average 16 wt%, which is lower than the 23 wt% reported experimentally by Mi et al. [59] and matched by [5,12,13,20], although these latter authors use this value as a parameter to fine-tune the membrane model, i.e. it is a “forced result”. The hydrated membrane density depends on the what value for the width of the interface between the polymer and the water is considered, which as seen in Fig. 9 can be several (2–3) nanometers. Nonetheless, this property is consistently reported in most simulation works and varies from 1.278 g/cm^3 to 1.5 g/cm^3 [12]. Our data, calculated by not considering the interfacial region, suggests an average value of 1.37 g/cm^3 (raw data provided in the Supplementary material).

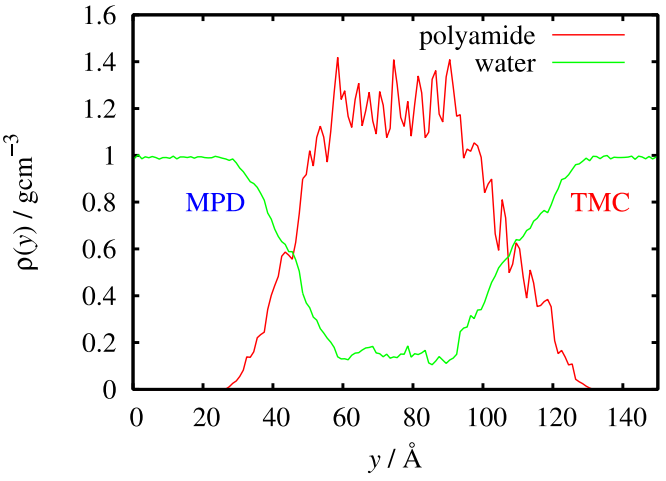

Fig. 9. Density profiles for a fully hydrated membrane shown in dry state in Fig. 7. Further profiles for other membrane realizations are supplied in the Supplementary material.

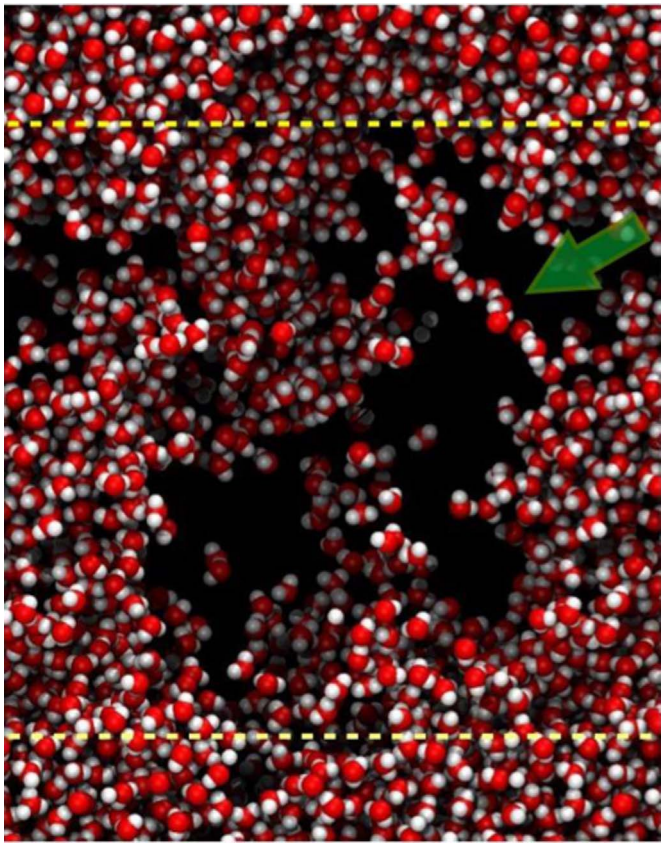

Fig. 10. Snapshot of an equilibrium configuration of a fully hydrated atomistic membrane. Only the water molecules are depicted (red are the oxygen atoms, white are the hydrogen atoms); the membrane atoms are made transparent. The top and bottom borders of the figure correspond to bulk liquid water domains. The membrane spans the width of the figure and the yellow dashed lines give indication of the interfase. Green arrow highlights a single-file of water molecules connecting larger water domains inside the membrane. (For interpretation of the references to color in this figure legend, the reader is referred to the web version of this article).

The pore structure of the membranes is highly irregular and it is misleading to describe it using the conventional pore size distribution measurements employed in the characterization of porous materials. It is likely that no single parameter can describe structural and transport properties alone [8]. We qualitatively observe a bimodal distribution of voids, with regions of strong confinement alongside regions where water is coordinated by other water molecules. These results add to the findings of Harder et al. [5] and of Kolev and Freger [8] which corroborate the bimodal distribution model proposed by Kim et al. [60]. Experimental analysis by Coronell et al. [61] also encounters a bimodal distribution of the dissociation constant of the carboxylic charges and interpret this as a marker of the different pathways available between very confined tight pores and more open liquid-filled voids.

Fig. 10 shows a snapshot of the water molecules within the polymer domain, where it is seen in the foreground that some water molecules find pathways across the membrane forming “conga-lines” [62] or single file diffusion pathways (*c.f.* highlight in Fig. 10). These instances have been described as responsible for unexpectedly high transport in carbon nanotube based systems [37]. There is a striking resemblance between our observations and the single-file pathways connecting small domains of bulk water that have been reported earlier [18]. However, the more salient feature in Fig. 10, which is shared with all other realizations of the atomistic membranes, is that there are fairly large pockets of water, not necessarily percolating both sides of the membrane, but contributing significantly to the water uptake. This seems to be a feature of the procedure used to generate the membrane,

i.e. it is a signature of the crosslinking nature of the polymer [27]. Our distribution of pores seems to have the same characteristics as those described by the tomographic in-plane stack maps of water density provided by Kolev and Freger [8]. It is possible that although larger pockets of bulk-like water are scattered around the membrane, the transport or percolation is limited by smaller and more restricted pores, some barely capable of sustaining a single file of water.

We calculate the self-diffusivity of water based on the Einstein equation, i.e. by evaluating the mean square diffusivity with respect to time [42] and we find a value of 3.4×10^{-6} cm^2/s for the diffusivity of water within the membrane. While the numerical result depends on the particular choice of water model and the particular realization of the membrane (see raw data in Supplementary material), it is observed that there is a decrease of an order of magnitude with respect to the corresponding value of the self-diffusivity of bulk water (2.5×10^{-5} cm^2/s at 300 K) [63]. These observations are consistent with the simulation results of Hughes et al. [18], Kolev and Freger [8] , Ding et al. [19] and Harder et al. [5] and the value of 1.7×10^{-6} cm^2/s obtained by quasi-elastic neutron scattering [64].

4.3. Comparison with experiments of Karan et al. [30]

An inherent limitation of the simulations is the size of the computational cell and the imposition of periodic boundary conditions parallel to the membrane. This limits the length scale of any structural features, such as surface roughness or undulations in the simulated membrane or the size of oligomer clusters prior to their incorporation in the membrane, to the computational cell size in the x and z directions, i.e. 5–10 nm. Thus, the simulations are unable to reproduce the crumpled membrane morphologies observed experimentally [30], where the lengths scales involved are between 100 and 500 nm. It was postulated [30] that the reason for the crumpling is that heat generated by the polymerization reaction causes Rayleigh-Bénard convection. However, in our simulations the temperature is maintained fairly constant through the use of Langevin dynamics, precluding such effects.

The recent paper by Karan et al. [30] reports the synthesis of free-standing, smooth PA membranes of thickness less than 10 nm, the properties of which can be compared to simulation. The simulations reported here have all assumed a concentration of MPD of 2 wt% in a virtual aqueous solution, which is within the range of concentrations of MPD studied experimentally by Karan et al. The largest ratio of MPD:TMC concentrations considered here is 3:1. By contrast, in the experiments of Karan et al. that ratio is 20:1. It is very unlikely that spanning clusters would be formed with a concentration ratio of 20:1 in the time we are able to simulate, which is about 0.1 μs. By contrast, the reactions in the experiments [30] proceed for seconds and minutes.

The surface roughnesses of the membranes shown in Figs. 7 and S3–S8 in the Supplementary material are comparable to those reported by Karan et al. [30] for their smooth (i.e. not crumpled films) films. However, the roughnesses reported by Karan et al. include contributions from the support membrane, so it is difficult to make a direct comparison. The thicknesses of the membranes simulated here of between 5 and 10 nm are in the same range as those reported experimentally [30] for their smooth films. This is a key indicator that the formation of the membrane by interfacial polymerization has been faithfully captured by the simulations.

For the smooth MPD-TMC film, with the concentration of MPD in the aqueous solution of 0.1 wt% and the concentration of TMC in hexane of 0.005 wt%, X-ray photoelectron spectroscopy measurements [30] revealed that after 1 minute the fraction of oxygen atoms in carboxyl groups was 26%, and the fraction of nitrogen atoms in amine groups was 5%. The remaining oxygen and nitrogen atoms were in amide bonds. Counting both oxygen atoms in each carboxyl group, it may be deduced from this data that there are approximately three times as many carboxyl groups in the experimental membranes as amine groups. For the membrane structures shown in Figs. 7 and S3–S8 in the Supplementary material, the average fraction of oxygen atoms in carboxyl groups is 11%, and the average fraction of nitrogen atoms in amine groups is 5%, with standard deviations of 3% and 1% respectively. On average there are about 20% more carboxyl groups in the simulated membranes than amine groups. There are no systematic variations for these fractions with the monomer concentration ratios. It is concluded that while it appears the amine group content of the simulated membranes is consistent with these experimental observations, the carboxyl group content is less than that observed experimentally by about a factor of 2.5. This discrepancy is surprising since the ratio of TMC:MPD monomer concentrations is greater in the simulations than in the experiments by about a factor of 7.

5. Conclusions

We have simulated the formation of PA membranes by a process that mimics interfacial polymerization of MPD and TMC monomers. These simulations have been made possible by two essential simplifications. First, we have developed coarse-grained representations of the monomers that reflect their stereochemistry and the planar conformation of the amide bond. Second, we avoid the explicit use of solvents for the monomers by allowing monomers to diffuse by Brownian motion. The resulting model membranes share some general characteristics (e.g. dry and hydrated densities, average transport properties) with atomistic models built on ad-hoc procedures, however, significant morphological differences are observed.

As in earlier studies we find the membrane forms through the growth and aggregation of oligomer clusters in the region occupied by the organic solvent. Before the oligomer clusters merge we find the unreacted acyl chloride and amine side groups are almost always on the surfaces of these clusters. When two clusters merge it is very difficult for the unreacted side groups on their surfaces to react either for steric reasons or because there is a preponderance of one type of side group. This leads to a reduced density of amide bonds at the interfaces between oligomer clusters when they are incorporated into the membrane. We found there are also significant density variations in the membrane and a non-uniform distribution of pores composed of tightly confined passages and larger bulk-like voids, consistent with inferences based on experimental results [60]. Chemical heterogeneities are also encountered with opposing concentration gradients of unreacted carboxyl and amine side groups in the membranes.

A comparison of the simulations with experiments of Karan et al. [30] is possible only for the smooth films found experimentally. The membrane thicknesses agree reasonably well, as does the surface roughness. The fraction of nitrogen atoms in amine side groups also agrees well. But the fraction of oxygen atoms in carboxyl groups is much less in the simulated films than is reported in the experimental films. The reason for this disagreement is not clear.

Acknowledgements

This work was supported by the BP International Centre for Advanced Materials. We are grateful to many members of the Molecular Systems Engineering group at Imperial College and BP for helpful discussions, the Imperial College High Performance Computing Service, and the Thomas Young Centre under Grant TYC-101.

Appendix A. Supplementary material

Supplementary data associated with this article can be found in the online version at http://dx.doi.org/10.1016/j.memsci.2016.11.024.

References

[1] D.S. Sholl, R.P. Lively, Seven chemical separations to change the world, Nature 532 (2016) 435–437.
[2] P.W. Morgan, Condensation Polymers: By Interfacial and Solution Methods 10, Interscience Publishers, 1965.
[3] A.K. Ghosh, B.-H. Jeong, X. Huang, E.M.V. Hoek, Impacts of reaction and curing conditions on polyamide composite reverse osmosis membrane properties, J. Membr. Sci. 311 (2008) 34–45.
[4] A.S. Barnard, In silico veritas, ACS Nano 8 (2014) 6520–6525.
[5] E.D. Harder, E. Walters, Y.D. Bodnar, R.S. Faibish, B. Roux, Molecular dynamics study of a polymeric reverse osmosis membrane, J. Phys. Chem B 113 (2009) 10177–10182.
[6] Y. Luo, E. Harder, R.S. Faibish, B. Roux, Computer simulations of water flux and salt permeability of the reverse osmosis FT-30 aromatic polyamide membrane, J. Membr. Sci. 384 (2011) 1–9.
[7] M. Shen, S. Keten, R.M. Lueptow, Dynamics of water and solute transport in polymeric reverse osmosis membranes via molecular dynamics simulations, J. Membr. Sci. 506 (2016) 95–108.
[8] V. Kolev, V. Freger, Hydration, porosity and water dynamics in the polyamide layer of reverse osmosis membranes: a molecular dynamics study, Polymer 55 (2014) 1420–1426.
[9] W. Tao, L. Zhang, H. Zhao, H. Ma, M.S.J. Sajib, H. Jiang, S. Murad, Aromatic polyamide reverse-osmosis membrane: an atomistic molecular dynamics simulation, J. Phys. Chem. B 120 (2016) 10311–10318.
[10] L.J. Abbott, K.E. Hart, C.M. Colina, Polymatic: a generalized simulated polymerization algorithm for amorphous polymers, Theor. Chem. Acc. 132 (2013) 1–19.
[11] L. Abbott, C. Colina, Polymatic: a simulated polymerization algorithm 1.0 (2015) Available at ⟨https://nanohub.org/resources/17278⟩.
[12] T.P. Liyana-Arachchi, J.F. Sturnfield, C.M. Colina, Ultrathin molecular-layer-by-layer polyamide membranes: insights from atomistic molecular simulations, J. Phys. Chem. B 120 (2016) 9484–9494.
[13] M.J. Kotelyanskii, N.J. Wagner, M.E. Paulaitis, Atomistic simulation of water and salt transport in the reverse osmosis membrane FT-30, J. Membr. Sci. 139 (1998) 1–16.
[14] M.J. Kotelyanskii, N.J. Wagner, M.E. Paulaitis, Molecular dynamics simulation study of the mechanisms of water diffusion in a hydrated, amorphous polyamide, Comput. Theor. Polym. Sci. 9 (1999) 301–306.
[15] W. Gao, F. She, J. Zhang, L.F. Dumée, L. He, P.D. Hodgson, L. Kong, Understanding water and ion transport behaviour and permeability through poly(amide) thin film composite membrane, J. Membr. Sci. 487 (2015) 32–39.
[16] X. Yuan, Y. Liu, B. Mi, Y. Leng, Hydrated polyamide membrane and its interaction with alginate: a molecular dynamics study, Langmuir 29 (2013) 11600–11608.
[17] X. Yuan, Y. Liu, B. Mi, Y. Leng, Molecular dynamics simulations of polyamide membrane, calcium alginate gel, and their interactions in aqueous solution, Langmuir 30 (2014) 9098–9106.
[18] Z.E. Hughes, J.D. Gale, A computational investigation of the properties of a reverse osmosis membrane, J. Mater. Chem. 20 (2010) 7788–7812.
[19] M. Ding, A. Ghoufi, A. Szymczyk, Molecular simulations of polyamide reverse osmosis membranes, Desalination 343 (2014) 48–53.
[20] M. Ding, A. Szymczyk, F. Goujon, A. Soldera, A. Ghoufi, Structure and dynamics of water confined in a polyamide reverse-osmosis membrane: a molecular-simulation study, J. Membr. Sci. 458 (2014) 236–244.
[21] M. Ding, A. Szymczyk, A. Ghoufi, On the structure and rejection of ions by a polyamide membrane in pressure-driven molecular dynamics simulations, Desalination 368 (2015) 76–80.
[22] K.T. Thomson, K.E. Gubbins, Modeling structural morphology of microporous carbons by reverse Monte Carlo, Langmuir 16 (2000) 5761–5773.
[23] R. Salazar, L.D. Gelb, A computational study of the reconstruction of amorphous mesoporous materials from gas adsorption isotherms and structure factors via evolutionary optimization, Langmuir 23 (2007) 530–541.
[24] R. Nadler, S. Srebnik, Molecular simulation of polyamide synthesis by interfacial polymerization, J. Membr. Sci. 315 (2008) 100–105.
[25] A.V. Berezkin, Y.V. Kudryavtsev, Hybrid approach combining dissipative particle dynamics and finite-difference diffusion model: simulation of reactive polymer coupling and interfacial polymerization, J. Chem. Phys. 139 (2013) 154102.
[26] A.V. Berezkin, Y.V. Kudryavtsev, Linear interfacial polymerization: theory and simulations with dissipative particle dynamics, J. Chem. Phys. 141 (2014) 194906–194917.
[27] A.V. Berezkin, Y.V. Kudryavtsev, Effect of cross-linking on the structure and growth of polymer films prepared by interfacial polymerization, Langmuir 31 (2015) 12279–12290.
[28] V. Freger, Kinetics of film formation by interfacial polycondensation, Langmuir 21 (2005) 1884–1894.
[29] General discussion, Computing power revolution and new algorithms: GP- GPUs, clouds and more, Faraday Discuss. 169 (2014) 379–401.
[30] Z. Karan, S. Jiang, A.G. Livingston, Sub-10 nm polyamide nanofilms with ultrafast solvent transport for molecular separation, Science 348 (2015) 1347–1351.
[31] E.L. Wittbecker, P.W. Morgan, Interfacial polycondensation. I, J. Polym. Sci. 40 (1959) 289–297.
[32] P.W. Morgan, S.L. Kwolek, Interfacial polycondensation. ii. Fundamentals of polymer formation at liquid interfaces, J. Polym. Sci. 40 (1959) 299–327.
[33] M. Mulder, Basic Principles of Membrane Technology., 2nd ed., Kluwer Academic Publishers, Netherlands, 1997.
[34] J.E. Cadotte, R.J. Petersen, R.E. Larson, E.E. Erickson, A new thin film seawater composite reverse osmosis membrane, Desalination 32 (1980) 25–31.
[35] A. Shrivastava, I.A. Tomlinson, A. Roy, J.E. Johnson, S. Jons, C.V. Funk, L. Franklin, M. Peery, L.D. Madsen, E.B. Svedberg (Eds.), Dow Chemical: Materials Science Contributions to Membrane Production in Materials Research for Manufacturing: An Industrial Perspective of Turning Materials into New Products, Springer, New York City, 2016.
[36] R.W. Baker, Membrane Technology and Applications, 3rd ed., Wiley, New York City, 2012.
[37] J. Wang, D.S. Dlamini, A.K. Mishra, M.T.M. Pendergast, M.C.Y. Wong, B.B. Mamba, V. Freger, A.R.D. Verliefde, E.M.V. Hoek, A critical review of transport through osmotic membranes, J. Membr. Sci. 454 (2014) 516–537.
[38] A.D. Becke, Density-functional exchange-energy approximation with correct asymptotic behavior, Phys. Rev. A 38 (1988) 3098–3100.
[39] W. Lee, C. Yang, R.G. Parr, Development of the Colle-Salvetti correlation-energy formula into a functional of the electron density, Phys. Rev. B 37 (1988) 785–789.
[40] P.C. Hariharan, J.A. Pople, The influence of polarization functions on molecular orbital hydrogenation energies, Theor. Chim. Acta 28 (1973) 213–222.
[41] T. Lafitte, C. Avendaño, V. Papaioannou, A. Galindo, C.S. Adjiman, G. Jackson, E.A. Müller, SAFT-γ force field for the simulation of molecular fluids: 3. Coarse-grained models of benzene and hetero-group models of n-decylbenzene, Mol. Phys. 110 (2012) 1189–1203.
[42] M.P. Allen, D.J. Tildesley, Computer Simulation of Liquids, Oxford Science Publications, Oxford, 1987.
[43] C.S. Dias, C. Braga, N.A.M. Araujo, M.M. Telo da Gama, Relaxation dynamics of functionalized colloids on attractive substrates, Soft Matter 12 (2016) 1550–1557.
[44] I. Snook, The Langevin and Generalised Langevin Approach to the Dynamics of Atomic, Polymeric and Colloidal Systems, Elsevier, Netherlands, 2007.
[45] S. Plimpton, Fast parallel algorithms for short-range molecular dynamics, J. Comput. Phys. 117 (1995) 1–19.
[46] T.E. Faber, Fluid Dynamics for Physicists, Cambridge, 1995.
[47] J.H. Dymond, H.A. Øye, Viscosity of selected liquid n–alkanes, J. Phys. Chem. Ref. Data 23 (1994) 41–53.
[48] G.S. Heffelfinger, F. van Swol, Diffusion in Lennard-Jones fluids using dual control volume grand canonical molecular dynamics simulation (DCVGCMD), J. Chem. Phys. 100 (1994) 7548–7552.
[49] G.-Y. Chai, W.B. Krantz, Formation and characterization of polyamide membranes via interfacial polymerization, J. Membr. Sci. 93 (1994) 175–192.
[50] J. Wang, R.M. Wolf, J.W. Caldwell, P.A. Kollman, D.A. Case, Development and testing of a general AMBER force field, J. Comput. Chem. 25 (2004) 1157–1174.
[51] P. Meakin, Diffusion-limited aggregation in three dimensions: Results from a new cluster-cluster aggregation model, J. Colloid Interface Sci. 102 (1984) 491–504.
[52] Y.-N. Tang, C.Y. Kwon, J.O. Leckie, Effect of membrane chemistry and coating layer on physiochemical properties of thin film composite polyamide RO and NF membranes: I. FTIR and XPS characterization of polyamide and coating layer chemistry, Desalination 242 (2009) 149–167.
[53] B.J. Coronell, O. Mariñas, D.G. Cahill, Depth heterogeneity of fully aromatic polyamide active layers in reverse osmosis and nanofiltration membranes, Environ. Sci. Technol. 45 (2011) 4513–4520.
[54] C.C. Wamser, M.I. Gilbert, Detection of surface functional group asymmetry in interfacially-polymerized films by contact angle titrations, Langmuir 8 (1992) 1608–1614.
[55] S. Würschum, R. Herth, U. Brossmann, Diffusion in nanocrystalline metals and alloys – a status report, Adv. Eng. Mater. 5 (2003) 365–372.
[56] V. Oizerovich-Honig, R. Raim, S. Srebnik, Simulation of thin film membranes formed by interfacial polymerization, Langmuir 26 (2010) 299–306.
[57] X. Zhang, D.G. Cahill, O. Coronell, B.J. Mariñas, Absorption of water in the active layer of reverse osmosis membranes, J. Membr. Sci. 331 (2009) 143–151.
[58] H.J.C. Berendsen, J.R. Grigera, T.P. Straatsma, The missing term in effective pair potentials, J. Phys. Chem. 91 (1987) 6269–6271 (1987).
[59] B. Mi, D.G. Cahill, B.J. Marinas, Physico-chemical integrity of nanofiltration/ reverse osmosis membranes during characterization by Rutherford backscattering spectrometry, J. Membr. Sci. 291 (2007) 77–85.
[60] S.H. Kim, S.-Y. Kwak, T. Suzuki, Positron annihilation spectroscopic evidence to demonstrate the flux-enhancement mechanism in morphology-controlled thin-film-composite (TFC) membrane, Environ. Sci. Technol. 39 (2005) 1764–1770.
[61] O. Coronell, M.I. González, B.J. Mariñas, D.G. Cahill, Ionization behavior, stoichiometry of association and accessibility of functional groups in the active layers of reverse osmosis and nanofiltration membranes, Environ. Sci. Technol. 44 (2010) 6808–6814.
[62] E.A. Müller, Purification of water through nanoporous carbon membranes: a molecular simulation viewpoint, Curr. Opin. Chem. Eng. 2 (2013) 223–228.
[63] H.J.C. Berendsen, J.R. Grigera, T.P. Straatsma, The missing term in effective pair potentials, J. Phys. Chem. 91 (1987) 6269–6271.
[64] Joao Cabral, Fabrizia Foglia, Personal Communication – Unpublished Results.